Nuclear Inst. and Methods in Physics Research, A 889 (2018) 138–144

Contents lists available at ScienceDirect

Nuclear Inst. and Methods in Physics Research, A

journal homepage: www.elsevier.com/locate/nima

Preparation and characterization of three ^{7}Be targets for the measurement of the ^{7}Be(n, p)^{7}Li and ^{7}Be(n, α)^{7}Li reaction cross sections

E.A. Maugeri [a,*], S. Heinitz [a], R. Dressler [a], M. Barbagallo [b], J. Ulrich [a], D. Schumann [a], N. Colonna [b], U. Köster [c], M. Ayranov [e], P. Vontobel [f], M. Mastromarco [b], J. Schell [d,g], J. Martins Correia [d], T. Stora [d], The n_TOF collaboration

[a] Laboratory of Radiochemistry, Paul Scherrer Institut, 5232 Villigen PSI, Switzerland
[b] Istituto Nazionale Fisica Nucleare—Sezione di Bari, Via E. Orabona 4, 70125 Bari, Italy
[c] Institut Laue-Langevin, 71 avenue des Martyrs, F-38042 Grenoble Cedex 9, France
[d] ISOLDE, CERN, CH-1211 Geneva 23, Switzerland
[e] European Commission, DG-Energy, 10 rue Rober Stumper, 2557 Luxembourg City, Luxembourg
[f] Laboratory for Neutron Scattering and Imaging, Paul Scherrer Institut, 5232 Villigen PSI, Switzerland
[g] Institute for Materials Science and Center for Nanointegration Duisburg–Essen (CENIDE), University of Duisburg–Essen, 45141 Essen, Germany

ARTICLE INFO

Keywords:
^{7}Be
Targets
Ion implanting
Radiographic imaging
ISOLDE-CERN
"Cosmological Lithium problem"
Neutron cross sections
n_TOF

ABSTRACT

This manuscript describes the production of three targets obtained by implantation of different activities of ^{7}Be into thin aluminium disks. Two of the produced targets were used to measure the ^{7}Be(n, p)^{7}Li cross section in the energy range of interest for the Big-Bang Nucleosynthesis. A third target was used to measure the cross sections of ^{7}Be(n, p)^{7}Li and ^{7}Be(n, α)^{7}Li nuclear reactions with cold and thermal neutrons, respectively. This paper describes also the characterization of the first two targets, performed after the neutron irradiation, in terms of implanted ^{7}Be activities and spatial distributions.

1. Introduction

Big-Bang Nucleosynthesis (BBN) is a theory that describes the chemical evolution of the Universe during the first minutes after the Big-Bang, when the temperature was low enough, between 100 keV and 10 keV, to let baryons to combine and to form isotopes of the light elements, up to Be; for a comprehensive overview see the section "Astrophysics and Cosmology" of [1] and references therein. The abundances of these isotopes can be calculated provided that the thermodynamics and the rate of the nuclear reactions involved in the process are known. To this end, the nuclear physics inputs, i.e. the nuclear cross sections, are a fundamental ingredient to calculate the primordial abundances and compare them with the observationally determined values. A very good agreement between predictions and observational data was obtained for ^{2}H [2] and ^{4}He [3], while the predicted abundance of ^{7}Li is a factor of 2–3 higher than the observed values in the atmosphere of low-metallicity stars in the Galactic halo [4,5]. This discrepancy represents one of the most debated and still unresolved issue in nuclear astrophysics and it is referred to for several decades as the "Cosmological Lithium problem" [6,7]. This discrepancy can be ascribed to one of following reasons: (1) systematic errors in the observation of light elements; (2) not well understood BBN physics; (3) inaccuracy of nuclear data. Before considering new physics beyond the Standard Model, it is worthwhile to re-evaluate the nuclear physics inputs used for the BBN calculations. Approximately 90%–95% of the primordial ^{7}Li (^{7}Li$_{prim}$) was generated from the electron capture decay of ^{7}Be [8,9]. Thus, the production/destruction rate of ^{7}Be determines the abundance of ^{7}Li$_{prim}$. While the production cross sections have been remeasured recently with very low uncertainty [10–13], the same cannot be said for the destruction rate. During the BBN most of ^{7}Be was destroyed via the ^{7}Be(n, p)^{7}Li(p, α)^{4}He reaction chain, with ^{7}Be(n, α)^{4}He considered to be the second most important reaction. The cross section of the latter reaction was recently measured for the first time between 0.01 eV and 10 keV neutron energy, partially covering the BBN energy [14]. The results indicate a minimum contribution of this reaction to the total destruction rate of ^{7}Be and, thus, do not solve the ^{7}Li$_{prim}$ discrepancy.

The ^{7}Be(n, p)^{7}Li cross section was measured in 1987 in the energy range from 0.025 eV to 13.5 keV [15], covering to some extent the range of BBN energy (10–100 keV). The cross sections at higher energies is

* Corresponding author.
E-mail address: emilio-andrea.maugeri@psi.ch (E.A. Maugeri).

https://doi.org/10.1016/j.nima.2018.01.078
Received 18 December 2017; Received in revised form 19 January 2018; Accepted 23 January 2018
Available online 3 February 2018

inferred from the time-reversal ^{7}Li(p, n)^{7}Be reaction, with a statistical error of about 0.7% [16] but, also in this case, leaving the cosmological lithium problem unsolved. However, direct measurements at higher neutron energy, up to 200 keV, are needed to exclude the presence of missed resonances that could drastically enhance the destruction rate of ^{7}Be.

For this reason, an international project aimed to measure the cross section of the ^{7}Be(n, p)^{7}Li reaction at neutron energy up to 300 keV, covering completely the BBN energy range, was started at the new high intensity neutron flux experimental area (EAR2) [17] of the Neutron Time-of-Flight facility (n_TOF) [18] at CERN, Switzerland. One of the issues of this measurement was the preparation and characterization of the ^{7}Be target. In order to minimize the energy loss of protons emitted in the ^{7}Be(n, p)^{7}Li reaction (Q-value 1.64 MeV), and suppress potential background related to neutron-induced reactions on other isotopes, the target material had to be as pure as possible and homogeneously distributed in a thin layer. Implantation of mass separated ^{7}Be appeared to be the best technique to produce targets with suitable purity and homogeneity.

The ion implantation technique had already been used before at the ISOLDE-CERN facility for implanting ^{7}Be, produced either on-line or off-line, into different materials. In on-line mode the ^{7}Be was produced by 1.4 GeV proton induced spallation in uranium carbide or graphite targets, respectively [19–21]. The maximum beam intensity for ^{7}Be was about 4×10^{9} ions/s from UC_x targets and 2.8×10^{10} ions/s with a 73 g/cm^2 thick graphite target in a special 40 cm long target container and 2 μA average proton current [20]. The on-line method reaches its limits when more than 10^{16} ^{7}Be atoms have to be implanted, like in the present application, and it becomes more efficient to perform the implantation in off-line mode using ^{7}Be produced elsewhere. A much more intense ^{7}Be beam, up to $\sim 2 \times 10^{12}$ ions/s, was generated off-line [22–27]. In this case ^{7}Be was extracted from a graphite target bombarded with 2 mA of 590 MeV protons for the production of pion and muon beams at Paul Scherrer Institute (PSI) [28]. The off-line method has one disadvantage: spallation reactions produce not only ^{7}Be but also ^{7}Li, that gets surface-ionized in the hot ion source and cannot be easily mass-separated from ^{7}Be. Therefore, on-line collections lead to co-implantation of non-negligible amounts of ^{7}Li. In off-line implantations ^{7}Li contamination can be considerably reduced by a chemical Li/Be separation prior to implantation or by “out-gassing” of the more volatile lithium before heating to implant beryllium.

The problem of this method is related to the availability of the irradiated graphite targets. In fact, these targets become available only when they are replaced with new ones, a procedure that takes place once every two to three years. For this reason Schumann et al. developed a different method for obtaining hundreds GBq of chemically pure ^{7}Be from the cooling water of the Spallation Induced Neutron Source (SINQ) facility at PSI, up to three times per year [29]. The latter method was followed in this work for obtaining ^{7}Be, which was implanted off-line in three distinct aluminium foils. Two of the obtained targets were used for the measurement of the ^{7}Be(n, p)^{7}Li reaction from cold neutron energies around 10 meV to intermediate neutron energies up to 300 keV at n_TOF-CERN. After the cross section measurements, the targets were investigated at PSI to determine the activity and spatial distribution of ^{7}Be, which, together with the knowledge of the neutron beam profile, is crucial for a correct evaluation of the cross sections. A third target was used for the measurement of the cross sections of ^{7}Be(n, p)^{7}Li and ^{7}Be(n, α)^{7}Li with cold and thermal neutrons respectively at ILL Grenoble and NPI Řež, respectively.

2. Experimental set-ups and methods

2.1. Preparation of the starting ^{7}Be material

Beryllium isotopes (^{7,9,10}Be) are produced in the cooling water of the SINQ facility at PSI by proton spallation reactions on ^{16}O. An ion exchange filter (LEWATIT mixed bed; Bayer, Canada) was used to extract Be^{2+}, with other cations present, from the cooling water. A second and more refined chemical separation was performed using the method described in [29,30] to obtain chemically pure beryllium in diluted HNO_3 solution. About 90 GBq of ^{7}Be were taken from the resulting solution and then loaded into a cylindrical graphite crucible, Fig. 1, in a lead shielded manipulator box, and heated at 333 K until dryness.

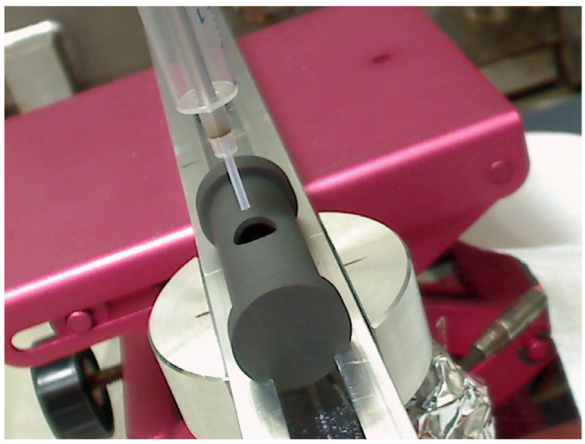

Fig. 1. Graphite crucible used to load the beryllium solution.

Afterwards, the crucible was transferred to the shielded hot cell of the ATEC facility at PSI, where, using remote controlled manipulators, it was inserted into the empty tantalum target container (20 mm inner diameter and 200 mm length) connected to a FEBIAD ion source unit equipped with a tantalum ionizer tube (3 mm inner diameter, 30 mm length). After being loaded with the ^{7}Be sample, the Ta container was sealed with a Ta plug, the surrounding vacuum chamber was closed and the entire unit was then placed into a lead shielded transport container and transferred to the ISOLDE facility at CERN in an identical manner as described in [28].

2.2. Implantation of ^{7}Be into aluminium foils

At CERN the unit containing the ^{7}Be sample was placed on the frontend of the ISOLDE General Purpose Separator (GPS), pumped to secondary vacuum, and both ionizer and target container were heated up to 1673 K for one day to outgas surface ionized impurities (Li, Na, Al, K, Ca, etc.…) present in the unit. Then the ionizer was heated to 2373 K, and the target container with the ^{7}Be sample was heated progressively from 1673 K to 1873 K. Beryllium was ionized via a two-step laser ionization scheme utilizing two ultraviolet transitions to an auto-ionizing state. The first step transition (234.9 nm) was generated by third harmonic generation of a red dye laser beam and the second step transition by second harmonic generation of a yellow dye laser beam. Both dye lasers were simultaneously pumped with the 532 nm frequency doubled output of a Nd:YAG laser operating at 10 kHz repetition rate. The generated ions were accelerated to 30 keV and mass-separated with the GPS. The mass 7 ion beam was then implanted into an aluminium backings, 1 in Fig. 2 (dimensions $h \times w \times d$ in mm: $50 \times 50 \times 0.018$), placed between two aluminium frames, 2 in Fig. 2 (dimensions $h \times w \times d$ in mm: $50 \times 50 \times 1$) with a 40 mm diameter central hole. The target was placed in a target holder, 3 in Fig. 2, specifically designed to facilitate insertion and extraction of the radioactive sample.

The first ^{7}Be sample for n_TOF (hereafter Target_22 MBq) was implanted into an aluminium backing on 12 April 2016. 1.47×10^{14} ^{7}Be ions, corresponding to an activity of about 22 MBq, were estimated to be implanted over 10 h. The ^{7}Be beam intensity was between 0.15 nA and 3 nA during the implantation. Comparing measurements of the ion

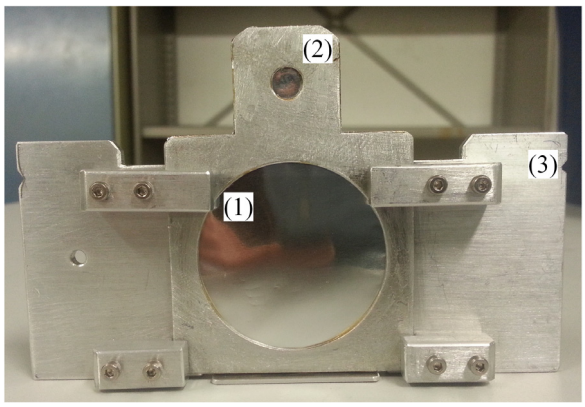

Fig. 2. Target assembly: (1) aluminium backings; (2) aluminium frame, (3) target holder.

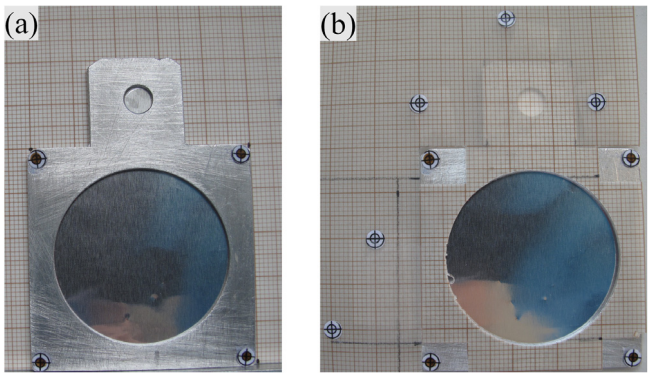

Fig. 3. Panel (a): Target_1 GBq consisting of an aluminium frame and an aluminium foil where ^{7}Be was implanted. Four spots of radioactive markers at the edges of the aluminium frame are used to establish an absolute coordinate system. Panel (b): Target_1 GBq placed behind a millimetre graph paper. The holes in the millimetre graph paper at the corresponding positions of the radioactive parts prevent the attenuation of emitted β-particles.

current while the resonance ionization lasers were switched on ("laser on" i.e. Be as well as Li isotopes were ionized) and switched off ("laser off" only Li isotopes can be ionized) showed that $^{7}Be^{+}$ represented 80% to 95% of the mass 7 beam, the remaining part originated from surface ionized $^{7}Li^{+}$.

After implantation of the first sample the target unit was cooled and placed in storage. Five weeks later it was placed back on the GPS frontend, reheated and outgassed for 24 h at temperatures up to 1673 K, but also accidentally for one hour up to 2223 K which probably caused the loss of a major part of the ^{7}Be sample contained in the graphite crucible.

The second ^{7}Be sample for n_TOF (hereafter Target_1 GBq) was implanted into an aluminium backing on 14 May 2016. The implantation procedure was the same as for the first target. In this case 7.2×10^{15} ions, corresponding to an activity of about 1 GBq, were estimated to be implanted over 10 h. The ^{7}Be beam intensity was between 5 nA and 44 nA during the implantation while heating the target from 1573 K to 1873 K. "Laser on" versus "laser off" measurements showed that $^{7}Be^{+}$ represented 99% of the mass 7 beam, the remaining 1% being surface ionized $^{7}Li^{+}$. These two targets were used for the n_TOF measurements.

A third ^{7}Be sample for the ILL Grenoble and NPI Řež collaboration was implanted into a 1.5 μm thin aluminium foil held in an aluminium frame on 14 May 2016. Over 98% of the beam was focused through a 5 mm diameter diaphragm. 5.0×10^{15} ions, corresponding to an activity of about 0.75 GBq, were estimated to be implanted over 8.5 h. The ^{7}Be beam intensity was between 11 nA and 42 nA during implantation while heating the target from 1873 K to 2033 K. 99% of the beam was $^{7}Be^{+}$ and 1% $^{7}Li^{+}$.

2.3. Characterization of the n_TOF ^{7}Be targets

Target_22 MBq and Target_1 GBq were then irradiated with neutrons at n_TOF, where the (n, p) reaction was measured as a function of the neutron energy. Afterwards, both targets were sent back to PSI where the total activity and distribution of the implanted ^{7}Be were measured.

2.3.1. Activity measurement

The activity of ^{7}Be of Target_22 MBq was measured on 17 March 2017, by means of a coaxial HPGe-detector (crystal dimensions: 35 mm diameter and 52 mm length) with a relative efficiency of 12% and providing an energy resolution of 1.77 keV at 1333 keV, in combination with Canberra modules for high-voltage supply, spectroscopy amplification and a 100 MHz Wilkinson 8192 channel ADC. The Genie2000® software package was used to analyse the obtained data. The distance between Target_22 MBq and the detector endcap (11 cm) was large enough to consider coincidence summing effects negligible. The value of activity was derived via comparison with a certified standard reference point source ^{152}Eu placed at the same distance in front of the detector. The same system and method were used for the ^{7}Be activity measurement of Target_1 GBq on 15 July 2016. In this case, due to the higher activity, the target was placed at 389 cm from the detector in order to keep the total impulse rate on the measurement chain on a reasonable range.

2.3.2. ^{7}Be distribution measurement

The ^{7}Be distribution was measured following two different methods: radiographic imaging (RI) and semi-automatic γ-scanning (GS), the latter was entirely developed in our laboratories.

2.3.2.1. Radiographic imaging. RI method was used to measure the spatial ^{7}Be distribution of both targets. In particular, a GE Typhoon™ FLA 7000 Imaging Plate Reader with spatial resolution down to 25 μm was used in combination with reusable Fujifilm imaging plates (IP) BAS-SR.

Fig. 3(a) shows a photograph of Target_1 GBq representative of Target_22 MBq as well. Four point-like sources of about 50 Bq of ^{44}Ti were placed at the edges of one aluminium frame. Those markers were used to link the relative obtained coordinates of RI to the geometrical centre of the target.

The target was placed on a millimetre graph paper with openings corresponding to the central hole of the aluminium frame and to the four ^{44}Ti markers, Fig. 3(b). An additional five ^{44}Ti markers were added onto the millimetre paper to improve the accuracy of the established absolute coordinates.

The implanted area of the targets was placed facing the imaging plate in a light-tight aluminium case. The recorded 2-dimensional RI-data display the locally accumulated energy dose deposited by photons or electrons. The reconstruction of the true ^{7}Be activity distribution was determined by a three step procedure. First, the recorded spacial activity distributions with a resolution of 25 μm were shrunk by summing subarrays of 10×10 measured data points in x- and y-direction producing a sampled down distribution with a 0.25 mm × 0.25 mm resolution. This in addition to reducing the image noise, reduced the dimensions of the images to a level suitable to apply image processing algorithms. In the second step a further enhancement of the signal quality was achieved by using a total variation filter assuming a Poisson like noise signal. A general feature of image processing procedures especially for noise reduction is an additional soft-focus of the picture and increase width of peak like distributions. The used regularization parameter of 0.25 was choose to enlarge the distribution width less than 5% as was checked with Monte-Carlo simulations [31].

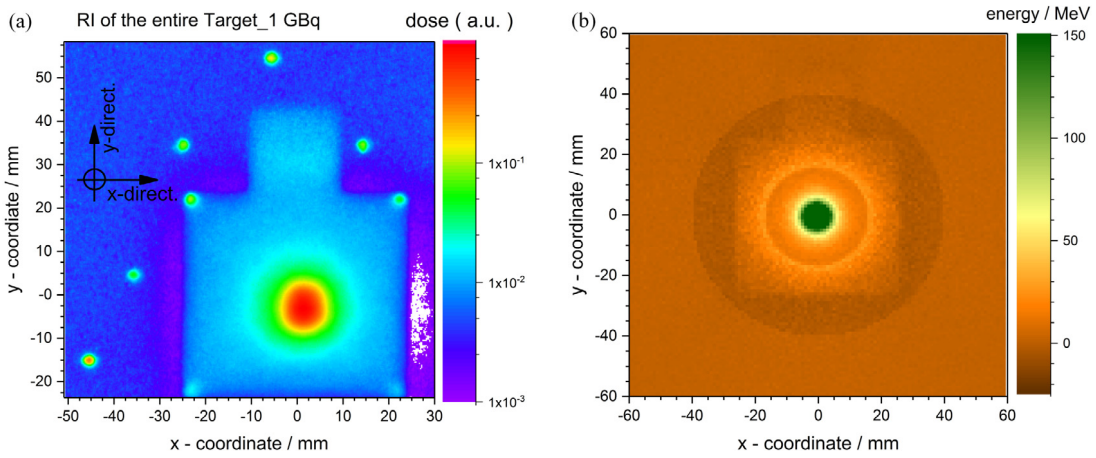

Fig. 4. Panel (a): Two-dimensional radiographic image of Target_1 GBq. Panel (b): GEANT4 simulation of the deposited energy in the IP after exposing with 477 keV γ-rays.

In the final step the blurring of the picture and spreading of the activity distribution due to the imaging process was reduced using an image deconvolution with steepest descent filter. The general shape of the point spread function was expected to be a Cauchy–Lorentz distribution displaying the one-over-r-squared law. The distance of the source activity to the IP was chosen as 1.2 mm, taking into account additional spacing of the graph paper and the internal structure of the IP [32].

In the case of the γ-scanning image no blurring effects were expected. Therefore, only a low-pass two dimensional fast Fourier transformation filter using a Gaussian window function with a cut-off frequency of 0.31 [1/pixel] was applied to reduce high frequency noise. The distribution parameters for all images were estimated afterwards by non-linear fitting a general two dimensional Gaussian distribution with an additional tilt parameter with respect to the y-axes to the filtered data.

2.3.2.2. Semi-automatic γ-scanning. The RI method is not suitable for targets with activity higher than several tens of MBq since, due to the high sensitivity of the IP, the signal will get saturated. Thus, in order to investigate Target_1 GBq, it was necessary to wait for more than one year, when its activity decayed to few MBq.

In that particular case due to the relatively short half-life of ^{7}Be ($t_{1/2}$ (53.22 ± 0.06) days [33]), it was possible to wait for ^{7}Be to decay to an optimum activity within a still reasonable for the project time frame. Nevertheless, this method cannot be used for targets of longer half-life isotopes with similar or higher activity than the initial activity of Target_1 GBq. This inspired the development of a new set-up, based on a semi-automatic γ-scanning system, to investigate activity distribution of highly active samples (from activities of few MBq up to activities higher than some GBq). This set-up was used to measure the ^{7}Be distribution of Target_1 GBq about three months after the ^{7}Be implantation, when its activity was still about 0.3 GBq. In particular, Target_1 GBq was placed in a 3D positioning system, which allowed precise movement (±0.01 mm), in front of a coaxial HPGe-detector. A 10 cm thick lead collimator with a 2 mm diameter aperture hole was placed between the target and the HPGe-detector. The distance between the target and the detector endcap was 32.4 cm. The geometrical centre of the target was aligned with the 2 mm aperture hole and with the centre of the detector using a laser pointer. The target was moved along the x- and y-axes by 2 mm steps. A total target area of 4 cm^2 was investigated, counting 121 individually measured points. 12 additional measurements were done with 1 mm step size around the deduced centre of the activity distribution, to improve the spatial resolution. The resolution of the obtained distribution is imposed by the aperture size of 2 mm.

The spatial reconstruction of the activity distribution with an up-scaled resolution of 0.25 mm × 0.25 mm using the Kriging algorithm [34,35] was achieved by applying the (radius/smoothing) parameters to the measured count rates. Afterwards, the distribution parameters were estimated with the same non-linear fitting procedure as described above.

The resulting ^{7}Be distribution was compared with the distribution obtained about one year later using RI, to validate the accuracy of the developed set-up.

3. Results and discussion

The ^{7}Be activity of Target_22 MBq was measured as (0.26 ± 0.04) MBq on 17 March 2017 ((21.6 ± 0.4) MBq referred to date of its implantation, 12 April 2016). The measured ^{7}Be activity of Target_1 GBq was (0.46 ± 0.02) GBq on 15 July 2016, corresponding to (1.03 ± 0.02) GBq referred to the date of its implantation, 14 May 2016.

Fig. 4(a) shows the RI of the entire Target_1 GBq set-up including the ^{44}Ti markers. In this case the IP was exposed to the implanted area for 40 min. After that, the implanted area was shielded with an aluminium plate, and the IP was exposed to the rest of the target (not implanted backing and frame) for other 200 min. Thus the IP was exposed to the not implanted part of the target for 240 min. The origin of the established coordinate system coincides with the geometrical centre of the target.

The area with higher dose (bright coloured region) represents the direct projection of the implanted area due to the primary photons 477.6 keV, emitted following ^{7}Be electron capture decay to the excited state of ^{7}Li (branching ratio 10.44%). While the photons scattered by both backing and frame impinging on the IP result in the entire target image (light blue area in Fig. 4(a)). This image, together with the ^{44}Ti markers, allows a perfect representation of the entire target geometry and, more importantly, to pinpoint the implanted area in respect to the geometrical centre of the target itself.

A simulation study with the GEANT4 toolkit (v10.3) [36] was performed to investigate whether or not the clearly visible shape of the target on the RI pictures is produced by scattering of the ^{7}Be decay radiation on both backing and target frame and does not have other origins such as contamination or activation of the sample frame.

The geometry of the aluminium backing and its holding frame was modelled using the given dimensions (see Section 2.3.2.1). In addition, a model of the imaging plate consisting of five various material layers was introduced; the layer thicknesses and compositions were modelled according to the data published in [37]. The implanted ^{7}Be activity was simplified as an ideal point source located in the geometrical centre of the aluminium foil, in a depth of 100 nm below the surface. In total 1.5 billion emitted gamma-rays with energy of 477 keV and an isotropic angular distribution were created and tracked through the entire sample geometry, corresponding roughly to a 240 min timeframe of exposure in the case of the autoradiography of Target_1 GBq. The accumulated

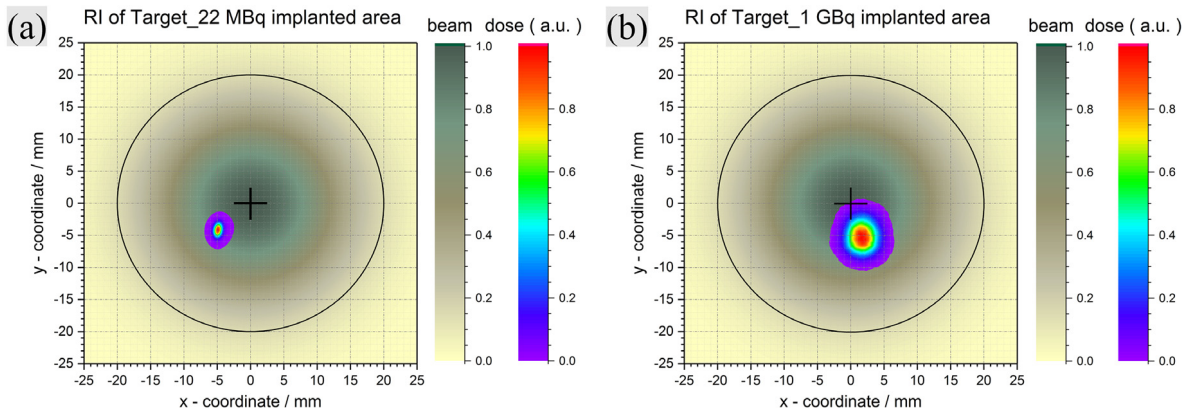

Fig. 5. Panel (a): 2D spatial reconstruction of the ^{7}Be distribution (right colour code) of the Target_22 MBq and Target_1 GBq, panel (a) and (b), respectively. Superimposed are the expected neutron field at EAR-2 (left colour code) and the geometrical centre of the target frame (black cross). All 2D distributions are normalized to the respective maximum. The RI data were down scaled to a resolution of 0.25 mm × 0.25 mm and filtered using a low pass 2D FFT Gaussian Filter. (For interpretation of the references to colour in this figure legend, the reader is referred to the web version of this article.)

Table 1
Position (in respect to the geometrical centre of the target) and width parameters of Target_22 MBq and Target_1 GBq.

Target Name	*x*-centre [mm]	*x*-width [mm]	*y*-centre [mm]	*y*-width [mm]	rotation [°]
RI of Target_22 MBq	−4.978 ± 0.008*	1.006 ± 0.006	−4.252 ± 0.012*	1.263 ± 0.011	−0.14
RI of Target_1 GBq	−1.699 ± 0.183*	2.064 ± 0.011	−5.200 ± 0.112*	2.440 ± 0.012	0.13
GS of Target_1 GBq	0.940 ± 0.002**	1.861 ± 0.002	−1.880 ± 0.003**	2.375 ± 0.003	0.23

* An additional uncertainty of about 0.36 mm of the location, caused by the placing and the measuring of the relative position of the ^{44}Ti markers relative to the target frame, must be considered.

** This uncertainty is negligible in respect to the resolution of the used set-up, i.e. 2 mm, due to aperture hole size of the collimator.

energy deposition caused by all arriving radiation in the sensitive layer of the IP was quantified using an orthogonal mesh grid with resolution of 1 mm × 1 mm. The energy deposition grid was divided in equally thick 10 sublayers to account for the assumed exponential depth-dependence of the plate readout [37]. The results of the simulation can be seen in Fig. 4(b). The shape of the target frame produced by secondary radiation is clearly present in the simulated spatial dose distribution, reproducing the phenomena seen on the autoradiography image of the ^{7}Be targets.

The width parameters and implanted positions of both targets were extracted from the resulting plots. Those values are summarized in Table 1. The given uncertainties result solely from the non-linear fitting procedure and do not include any systematic uncertainties from the established coordinate system. The results indicate that the implanted area of both targets has a planar cross section of an ellipse, with the implanted area of Target_22 MBq more elongated (its eccentricity is closer to one) than the one of Target_1 GBq. The implanted area of Target_22 MBq is shifted with respect to the geometrical centre of the target. A different location of the implanted area was found for Target_1 GBq, i.e. a shift with respect to the geometrical centre of the respective target in an opposite direction compared with Target_22 MBq.

Fig. 5 shows the RI 2D graphs of Target_22 MBq and Target_1 GBq, panel (a) and (b), respectively, both superimposed to the n_TOF neutron beam profile (extrapolated from [38]) where the centre of the beam profile was overlapped to the geometrical centre of the target. It is possible to see that the implanted area of Target_22 MBq was exposed only to about 80% to 60% of the beam intensity while the implanted area of Target_1 GBq was exposed to about 85% to 75% of the neutron beam.

Fig. 6 presents the γ-scan obtained using the GS set-up, described in Section 2.3.2.2, of Target_1 GBq. Comparing the obtained distribution with the one of RI (see Table 1), it is possible to see that the developed set-up allowed us to identify the position of the implanted area within a margin smaller than the resolution of used set-up, i.e. 2 mm.

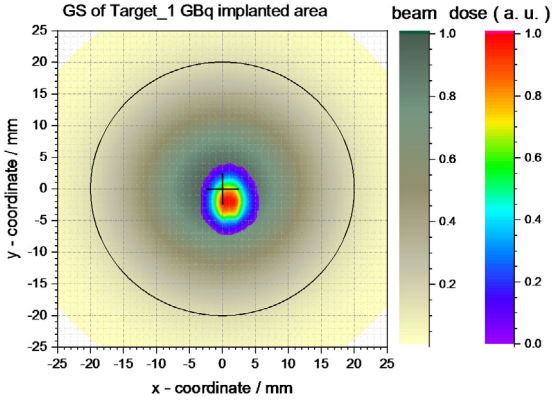

Fig. 6. GS of Target_1 GBq. The data were up scaled to a resolution of 0.25 mm × 0.25 mm using the Kriging algorithm.

4. Conclusions

For the first time, thanks to a well-established collaboration between PSI and CERN (ISOLDE and n_TOF), high activities of ^{7}Be were successfully implanted in three different thin aluminium foils to produce three targets, two of which were used for the measurement of the ^{7}Be(n, p)^{7}Li cross section in the energy range of interest for the BBN at EAR2 of n_TOF-CERN, while the third one was used for the measurement of the cross sections of ^{7}Be(n, p)^{7}Li and ^{7}Be(n, α)^{7}Li with cold and thermal neutrons in a collaboration between ILL Grenoble and NPI Řež, respectively. The activity of the first two targets was measured at PSI after the neutron irradiation, to be (21.6 ± 0.4) MBq and (1.03 ± 0.02) GBq, respectively. These results coincide very well with the data deduced from the total numbers of implanted ions during the ISOLDE runs. The implanted area of the two targets was characterized

in terms of position (in respect to the geometrical centre of the target) and width parameters by means of radiographic imaging method. The resulting positions were superimposed to the n_TOF neutron beam profile, allowing a more accurate determination of the cross sections. A semi-automatic gamma scanning system was set-up, allowing us to identify the activity distribution in targets of activity as high as 0.3 GBq with a resolution of 2 mm.

Acknowledgements

The work has partly been funded by CHANDA (grant agreement No FP7-Fission-2013-605203).

The Federal Ministry of Education and Research through the FMeV-grant 05K16PGA, has partially supported the use of the implantation equipment.

Appendix. The n_TOF collaboration

O. Aberle[1], V. Alcayne[2], J. Andrzejewski[3], L. Audouin[4], V. Bécares[2], M. Bacak[1,5,6], F. Bečvář[8], G. Bellia[9,10], E. Berthoumieux[6], J. Billowes[11], D. Bosnar[12], A. Brown[13], M. Busso[7,14,15], M. Caamaño[16], L. Caballero-Ontanaya[17], F. Calviño[18], M. Calviani[1], D. Cano-Ott[2], A. Casanovas[18], F. Cerutti[1], Y.H. Chen[4], E. Chiaveri[1,11,19], G. Cortés[18], M.A. Cortés-Giraldo[19], L. Cosentino[9], S. Cristallo[7,14,20], L.A. Damone[7,21], M. Diakaki[22,1], M. Dietz[23], C. Domingo-Pardo[17], E. Dupont[6], I. Durán[16], Z. Eleme[25], B. Fernández-Domínguez[16], A. Ferrari[1], P. Ferreira[26], P. Finocchiaro[9], V. Furman[27], K. Göbel[28], A. Gawlik[3], S. Gilardoni[1], T. Glodariu[29], I.F. Gonçalves[26], E. González-Romero[2], C. Guerrero[19], F. Gunsing[6], J. Heyse[30], D.G. Jenkins[13], F. Käppeler[31], Y. Kadi[1], T. Katabuchi[32], A. Kimura[33], N. Kivel[24], M. Kokkoris[22], Y. Kopatch[27], M. Krtička[8], D. Kurtulgil[28], I. Ladarescu[17], C. Lederer-Woods[23], J. Lerendegui-Marco[19], S. Lo Meo[34,35], S.J. Lonsdale[23], D. Macina[1], T. Martínez[2], A. Masi[1], C. Massimi[35,36], P. Mastinu[37], F. Matteucci[38,39], A. Mazzone[7,40], E. Mendoza[2], A. Mengoni[34], V. Michalopoulou[22], P. M. Milazzo[38], F. Mingrone[1], A. Musumarra[9,10], A. Negret[29], R. Nolte[41], F. Ogállar[42], A. Oprea[29], N. Patronis[25], A. Pavlik[43], J. Perkowski[3], L. Persanti[7,14,20], I. Porras[42], J. Praena[42], J. M. Quesada[19], D. Radeck[41], D. Ramos[4], T. Rauscher[44,23], R. Reifarth[28], D. Rochman[24], M. Sabaté-Gilarte[1,19], A. Saxena[45], P. Schillebeeckx[30], S. Simone[9], A.G. Smith[11], N.V. Sosnin[11], A. Stamatopoulos[22], G. Tagliente[7], J.L. Tain[17], T. Talip[24], A. Tarifeño-Saldivia[18], L. Tassan-Got[1,4], A. Tsinganis[1], S. Valenta[8], G. Vannini[35,36], V. Variale[7], P. Vaz[26], A. Ventura[35], V. Vlachoudis[1], R. Vlastou[22], A. Wallner[46], P.J. Woods[23], T. Wright[11], P. Žugec[12],

[1] European Organization for Nuclear Research (CERN), Switzerland
[2] Centro de Investigaciones Energéticas Medioambientales y Tecnológicas (CIEMAT), Spain
[3] University of Lodz, Poland
[4] Institut de Physique Nucléaire, CNRS-IN2P3, Univ. Paris-Sud, Université Paris-Saclay, F-91406 Orsay Cedex, France
[5] Technische Universität Wien, Austria
[6] CEA Irfu, Université Paris-Saclay, F-91191 Gif-sur-Yvette, France
[7] Istituto Nazionale di Fisica Nucleare, Sezione di Bari, Italy
[8] Charles University, Prague, Czech Republic
[9] INFN Laboratori Nazionali del Sud, Catania, Italy
[10] Dipartimento di Fisica e Astronomia, Università di Catania, Italy
[11] University of Manchester, United Kingdom
[12] Department of Physics, Faculty of Science, University of Zagreb, Zagreb, Croatia
[13] University of York, United Kingdom
[14] Istituto Nazionale di Fisica Nucleare, Sezione di Perugia, Italy
[15] Dipartimento di Fisica e Geologia, Università di Perugia, Italy
[16] University of Santiago de Compostela, Spain
[17] Instituto de Física Corpuscular, Universidad de Valencia, Spain
[18] Universitat Politècnica de Catalunya, Spain
[19] Universidad de Sevilla, Spain
[20] Istituto Nazionale di Astrofisica - Osservatorio Astronomico di Teramo, Italy
[21] Dipartimento di Fisica, Università degli Studi di Bari, Italy
[22] National Technical University of Athens, Greece
[23] School of Physics and Astronomy, University of Edinburgh, United Kingdom
[24] Paul Scherrer Institut (PSI), Villingen, Switzerland
[25] University of Ioannina, Greece
[26] Instituto Superior Técnico, Lisbon, Portugal
[27] Joint Institute for Nuclear Research (JINR), Dubna, Russia
[28] Goethe University Frankfurt, Germany
[29] Horia Hulubei National Institute of Physics and Nuclear Engineering, Romania
[30] European Commission, Joint Research Centre, Geel, Retieseweg 111, B-2440 Geel, Belgium
[31] Karlsruhe Institute of Technology, Campus North, IKP, 76021 Karlsruhe, Germany
[32] Tokyo Institute of Technology, Japan
[33] Japan Atomic Energy Agency (JAEA), Tokai-mura, Japan
[34] Agenzia nazionale per le nuove tecnologie (ENEA), Bologna, Italy
[35] Istituto Nazionale di Fisica Nucleare, Sezione di Bologna, Italy
[36] Dipartimento di Fisica e Astronomia, Università di Bologna, Italy
[37] Istituto Nazionale di Fisica Nucleare, Sezione di Legnaro, Italy
[38] Istituto Nazionale di Fisica Nucleare, Sezione di Trieste, Italy
[39] Dipartimento di Astronomia, Università di Trieste, Italy
[40] Consiglio Nazionale delle Ricerche, Bari, Italy
[41] Physikalisch-Technische Bundesanstalt (PTB), Bundesallee 100, 38116 Braunschweig, Germany
[42] University of Granada, Spain
[43] University of Vienna, Faculty of Physics, Vienna, Austria
[44] Department of Physics, University of Basel, Switzerland
[45] Bhabha Atomic Research Centre (BARC), India
[46] Australian National University, Canberra, Australia

References

[1] C. Patrignani, K. Agashe, G. Aielli, C. Amsler, M. Antonelli, D.M. Asner, H. Baer, S. Banerjee, R.M. Barnett, T. Basaglia, C.W. Bauer, J.J. Beatty, V.I. Belousov, et al., Review of particle physics, Chin. Phys. C 40 (2016).
[2] J.C. Ryan, P. Max, A.J. Regina, T.M. Michael, C.S. Charles, Precision measures of the primordial abundance of deuterium, Astrophys. J. 781 (2014) 31.
[3] E. Aver, K.A. Olive, E.D. Skillman, The effects of He I λ10830 on helium abundance determinations, J. Cosmol. Astropart. Phys. 7 (2015) 011.
[4] F. Spite, M. Spite, Abundance of lithium in unevolved halo stars and old disk stars: Interpretation and consequences, Astron. Astrophys. 115 (1982) 357.
[5] M. Asplund, D.L. Lambert, P.E. Nissen, F. Primas, V.V. Smith, Lithium isotopic abundances in metal-poor halo stars, Astrophys. J. 644 (2006) 229.
[6] G. Steigman, Primordial nucleosynthesis in the precision cosmology era, Annu. Rev. Nucl. Part. Sci. 57 (2007) 463.
[7] B.D. Fields, The primordial lithium problem, Annu. Rev. Nucl. Part. Sci. 61 (2011) 47.
[8] M. Pospelov, J. Pradler, Metastable GeV-scale particles as a solution to the cosmological lithium problem, Phys. Rev. D 82 (2010) 103514.
[9] R. Khatri, R.A. Sunyaev, Time of primordial ^{7}Be conversion into ^{7}Li, energy release and doublet of narrow cosmological neutrino lines, Astron. Lett. 37 (2011) 367.
[10] B.S.N. Singh, M. Hass, Y. Nir-El, G. Haquin, A New precision measurement of the ^{3}He(^{4}He, gamma)^{7}Be cross section, Nuclear Phys. A 758 (2005) 689.
[11] T.A.D. Brown, C. Bordeanu, K.A. Snover, D.W. Storm, D. Melconian, A.L. Sallaska, S.K.L. Sjue, S. Triambak, ^{3}He + ^{4}He $\rightarrow$ ^{7}Be astrophysical S factor, Phys. Rev. C 76 (2007) 055801.
[12] F. Confortola, D. Bemmerer, H. Costantini, A. Formicola, G. Gyürky, P. Bezzon, R. Bonetti, C. Broggini, P. Corvisiero, Z. Elekes, Z. Fülöp, G. Gervino, A. Guglielmetti, et al., Astrophysical S factor of the ^{3}He(α, γ)^{7}Be reaction measured at low energy via detection of prompt and delayed γ rays, Phys. Rev. C 75 (2007) 065803.
[13] G. Gyürky, F. Confortola, H. Costantini, A. Formicola, D. Bemmerer, R. Bonetti, C. Broggini, P. Corvisiero, Z. Elekes, Z. Fülöp, G. Gervino, A. Guglielmetti, C. Gustavino, et al., ^{3}He(α, γ)^{7}Be cross section at low energies, Phys. Rev. C 75 (2007) 035805.
[14] M. Barbagallo, A. Musumarra, L. Cosentino, E.A. Maugeri, S. Heinitz, A. Mengoni, R. Dressler, D. Schumann, F. Kaeppeler, N. Colonna, P. Finocchiaro, M. Ayranov, L. Damone, et al., The ^{7}Be(n, α)^{4}He reaction and the cosmological lithium problem: Measurement of the cross section in a wide energy range at n_TOF at CERN, Phys. Rev. Lett. 117 (2016) 152701.

[15] P.E. Koehler, C.D. Bowman, F.J. Steinkruger, D.C. Moody, G.M. Hale, J.W. Starner, S.A. Wender, R.C. Haight, P.W. Lisowski, W.L. Talbert, ^{7}Be(n, p)^{7}Li total cross section from 25 meV to 13.5 keV, Phys. Rev. C 37 (1988) 917.
[16] P.D. Serpico, S. Esposito, F. Iocco, G. Mangano, G. Miele, O. Pisanti, Nuclear reaction network for primordial nucleosynthesis: a detailed analysis of rates, uncertainties and light nuclei yields, J. Cosmol. Astropart. Phys. 12 (2004) 010.
[17] M. Sabaté-Gilarte, M. Barbagallo, N. Colonna, F. Gunsing, P. Žugec, V. Vlachoudis, Y.H. Chen, A. Stamatopoulos, J. Lerendegui-Marco, M.A. Cortés-Giraldo, A. Villacorta, C. Guerrero, L. Damone, et al., High-accuracy determination of the neutron flux in the new experimental area n_TOF-EAR2 at CERN, Eur. Phys. J. A 53 (2017) 210.
[18] C. Guerrero, A. Tsinganis, E. Berthoumieux, M. Barbagallo, F. Belloni, F. Gunsing, C. Weiss, E. Chiaveri, M. Calviani, V. Vlachoudis, S. Altstadt, S. Andriamonje, J. Andrzejewski, et al., Performance of the neutron time-of-flight facility n_TOF at CERN, Eur. Phys. J. A 49 (2013) 27.
[19] O. Koskelo, U. Koster, F. Tuomisto, K. Helariutta, M. Sopanen, S. Suihkonen, O. Svensk, J. Raisanen, Migration kinetics of ion-implanted beryllium in ZnO and GaN, Phys. Scr. 88 (2013) 035603.
[20] U. Koster, J. Barker, R. Catherall, V.N. Fedoseyev, U. Georg, G. Huber, Y. Jading, O. Jonsson, M. Koizumi, K.L. Kratz, E. Kugler, J. Lettry, V.I. Mishin, et al., On-line separation of short-lived beryllium isotopes, AIP Conf. Proc. 455 (1998) 989.
[21] C. Mazzocchi, Z. Janas, P. Baczyk, H.O.U. Fynbo, U. Koster, Precision half-life measurement of ^{7}Be implanted in different materials, Acta Phys. Polon. B 43 (2012) 279.
[22] M. Hass, C. Broude, V. Fedoseev, G. Goldring, G. Huber, J. Lettry, V. Mishin, H.J. Ravn, V. Sebastian, L. Weissman, I. Collaboration, A new measurement of the ^{7}Be$(p,\gamma)^{8}$B cross-section with an implanted ^{7}Be target, Phys. Lett. B 462 (1999) 237.
[23] L.T. Baby, C. Bordeanu, G. Goldring, M. Hass, L. Weissman, V.N. Fedoseyev, U. Köster, Y. Nir-El, G. Haquin, H.W. Gäggeler, R. Weinreich, New measurement of the proton capture rate on ^{7}Be and the S_{17} (0) factor, Phys. Rev. C 67 (2003) 065805.
[24] Y. Nir-El, G. Haquin, Z. Yungreiss, M. Hass, G. Goldring, S.K. Chamoli, B.S.N. Singh, S. Lakshmi, U. Koster, N. Champault, A. Dorsival, G. Georgiev, V.N. Fedoseyev, et al., Precision measurement of the decay rate of ^{7}Be in host materials, Phys. Rev. C 75 (2007).
[25] O. Koskelo, P. Pusa, J. Raisanen, U. Koster, I. Riihimaki, Diffusion of beryllium in Ge and Si–Ge alloys, J. Appl. Phys. 103 (2008) 073513.
[26] O. Koskelo, U. Koster, I. Riihimaki, J. Raisanen, Migration kinetics of ion-implanted beryllium in glassy carbon, Diam. Relat. Mater. 17 (2008) 1991.
[27] U. Koster, C. Granja, J. Jakubek, J. Uher, J. Vacik, Slow-neutron-induced charged-particle emission-channeling-measurements with Medipix detectors, Nucl. Instrum. Methods Phys. Res. A 633 (2011) S267.
[28] U. Köster, M. Argentini, R. Catherall, V.N. Fedoseyev, H.W. Gäggeler, O.C. Jonsson, R. Weinreich, Off-line production of intense ^{7,10}Be^{+} beams, Nucl. Instrum. Methods Phys. Res. B 204 (2003) 343.
[29] D. Schumann, M. Ayranov, T. Stowasser, L. Gialanella, A. di Leva, M. Romano, D. Schuermann, Radiochemical separation of ^{7}Be from the cooling water of the neutron spallation source SINQ at PSI, Radiochim. Acta 101 (2013) 509.
[30] E.A. Maugeri, S. Heinitz, R. Dressler, M. Barbagallo, N. Kivel, D. Schumann, M. Ayranov, A. Musumarra, M. Gai, N. Colonna, M. Paul, S. Halfon, L. Cosentino, et al., Preparation of ^{7}Be targets for nuclear astrophysics research, J. Instrum. 12 (2017) P02016.
[31] L.I. Rudin, S. Osher, E. Fatemi, Nonlinear total variation based noise removal algorithms, Physica D 60 (1992) 259.
[32] P.C. Hansen, J.G. Nagy, D.P. O'Leary, Deblurring Images: Matrices, Spectra, and Filtering, Society for Industrial and Applied Mathematics, Philadelphia, PA, USA, 2006.
[33] G. Audi, F.G. Kondev, M. Wang, B. Pfeiffer, X. Sun, J. Blachot, M. MacCormick, The NUBASE2012 evaluation of nuclear properties, Chin. Phys. C 36 (2012) 1157.
[34] D.G. Krige, A statistical approach to some mine valuation and allied problems on the Witwatersrand, J. Chem. Metal. Min. Soc. South Afr. 52 (1951) 119.
[35] S.I. Sakata, F. Ashida, M. Zako, Approximate structural optimization using Kriging method and digital modeling technique considering noise in sampling data, Comput. Struct. 86 (2008) 1477.
[36] S. Agostinelli, J. Allison, K. Amako, J. Apostolakis, H. Araujo, P. Arce, M. Asai, D. Axen, S. Banerjee, G. Barrand, F. Behner, L. Bellagamba, J. Boudreau, et al., Geant4 — a simulation toolkit, Nucl. Instrum. Methods Phys. Res. A 506 (2003) 250.
[37] N. Izumi, J. Lee, E. Romano, G. Stone, B. Maddox, T. Ma, V. Rekow, D.K. Bradley, P. Bell, X-ray and neutron sensitivity of imaging plates, in: SPIE Optical Engineering + Applications, SPIE, 2013, p. 8.
[38] C. Weiß, E. Chiaveri, S. Girod, V. Vlachoudis, O. Aberle, S. Barros, I. Bergström, E. Berthoumieux, M. Calviani, C. Guerrero, M. Sabaté-Gilarte, A. Tsinganis, J. Andrzejewski, et al., The new vertical neutron beam line at the CERN n_TOF facility design and outlook on the performance, Nucl. Instrum. Methods Phys. Res. A 799 (2015) 90.